Forward acceleration of ions from underdense plasma interactions with the Vulcan Petawatt laser

L Willingale, S P D Mangles, P M Nilson, Z Najmudin, M S Wei, A G R Thomas, M C Kaluza, A E Dangor, K Krushelnick
The Blackett Laboratory, Imperial College London, Prince Consort Road, London, SW7 2BW, UK

K L Lancaster, R J Clarke
Central Laser Facility, CCLRC Rutherford Appleton Laboratory, Chilton, Didcot, Oxon., OX11 0QX, UK

S Karsch, J Schreiber
Max-Planck-Institut für Quantenoptik, Hans-Kopfermann-Straße 1, D-85748 Garching, Germany

M Tatarakis
Technological Educational Institute of Crete, Chania, Crete, Greece

Main contact email address: *louise.willingale@imperial.ac.uk*

Introduction

With the development of short-pulse high-intensity lasers it has become possible to generate energetic particles from laser-plasma interactions, such as relativistic electrons[1)] and MeV ions[2)]. Laser-plasma interactions can be broadly generalized into either underdense or overdense interactions depending on whether or not the laser can propagate through the plasma. Previous investigations into overdense plasma ion acceleration use a solid target and a beam of ions is emitted from the front and rear surfaces[3)] which are generated by large space-charge fields at the target surfaces.

The focus of ion investigation from underdense plasma on the other hand has been on the transversely emitted ions at MeV energies[2)]. A 'Coulomb explosion[4)] accelerates these transverse ions through the large space-charge field generated by the expulsion of electrons from the central channel by the ponderomotive force of the laser. More recently, a collisionless shock acceleration mechanism has been observed to enhance the maximum energy of the transverse ions[5)]. Potential applications for collimated laser produced ion sources include ion fast ignitor schemes[6)]. They are already being effectively used for the radiography of laser-plasma interactions to diagnose the presence of electro-magnetic fields[7)].

Presented here are preliminary observations of MeV ions detected in the forward direction from underdense laser-plasma interactions. The observed ion beam has a maximum energy much higher than the transverse ion beam from the same interaction. Theory of forward ion acceleration regimes in underdense plasma has been considered, but suggests the generation of collimated beams of relativistic ions[8)]. In these experiments, longitudinally accelerated ions are generated in a similar way to those generated at the back surface of solid target interactions. The fast electrons leaving the plasma generate a large electric field, which pulls out ions producing a MeV ion beam. The fast electrons in this regime are accelerated to up to hundreds of MeV by a direct laser acceleration mechanism[9)].

Particle-in-cell (PIC) simulations were used to investigate the effect of the plasma density, the length of the density ramp and the laser parameters on the acceleration of the ions in the forward direction. A highly collimated beam of ions is seen in the simulations with a divergence of about a half angle of 5° at 20 MeV.

Experimental Set-up

This experiment was performed using the Vulcan Petawatt laser at the Rutherford Appleton Laboratory. The laser pulse had a full width half maximum (FWHM) duration of (1.0 ± 0.5) ps with energy of up to 343 J on target and has a central wavelength of 1.054 μm. An f/3 off-axis parabolic mirror focused the laser onto the edge of a gas jet with a 2 mm diameter supersonic nozzle with a focal spot FWHM diameter of 7 μm in vacuum. The maximum vacuum intensity of the laser was therefore 5.8×10^{20} Wcm^{-2}, which corresponds to a normalized vector potential, a_0, of 25. The backing pressure of the deuterium or helium gas to the gas-jet nozzle was varied so that the electron density of the plasma could be set at between $(0.7 – 4.0) \times 10^{19}$ cm^{-3}. The satellite frequencies of the forward Raman scattered laser spectra were used to calculate the electron plasma frequency, $\omega_{pe} = (n_e e^2/m_e \varepsilon_0)^{1/2}$, of the interaction where e is the charge on an electron, m_e is the mass of an electron and n_e is the electron density, which is then determined.

The ions were measured in the longitudinal direction, exactly on the laser axis, using the magnetic field of the electron spectrometer. The ions are deflected, in the opposite direction from the electrons, by an angle determined by how much energy they have and their mass to charge ratio. The energy resolution of the ion spectra was determined by the width of the entrance slit to the spectrometer, which was 2 mm wide. The nuclear track detector CR39 was used to detect the ions. For a helium gas target, there are two possible ions, He^{1+} and He^{2+}. These were distinguished by looking at the pit size at a particular deflection. A stronger force will be felt by a He^{2+} ion in the spectrometer so the deflection will be greater than for a He^{1+} ion with the same energy. Therefore, at a particular point on the detector, there could be both ion species present but the He^{2+} detected at this point would have had more energy. The higher the energy of an ion, the further into the CR39 it will travel before it is stopped and therefore the damage will be deeper into the material. When the CR39 is etched, pits appear where the ions are stopped and the deeper the damage goes the smaller the diameter of the pit. Hence at a particular point, the smaller pits will be from the He^{2+} ions and the large one from the He^{1+} ions and therefore they could be distinguished from one another.

Experimental Results

Presented here is a shot for which the laser had a vacuum intensity of 5.8×10^{20} Wcm^{-2} ($a_0 \sim 21.6$) into a helium plasma with an electron density of 4×10^{19} cm^{-3}. The electron spectrum for this shot has a maximum energy of around 60 MeV. The helium spectra for both the forward and the transverse direction are shown in Figure 1. In the transverse direction the He^{2+} had a maximum energy of (7.8 ± 0.6) MeV and the He^{1+} had a maximum energy of (3.4 ± 0.4) MeV. In the longitudinal direction the He^{2+} had a maximum energy of (51 ± 16) MeV and the He^{1+} had a maximum energy of (13 ± 4) MeV. The maximum energy helium ion detectable by the 1 mm thick CR39 should be 43 MeV. This is because when the CR39 is etched, a pit forms on the CR39 where an ion deposits enough energy, which always occurs just before the ion is stopped at the Bragg peak. Higher energy ions can travel further though the CR39 before they are stopped and deposit enough energy to damage the CR39 so that a pit will form during etching. If there were helium ions of the maximum

energy of 43 MeV then pits on the reverse of the detector should be visible. However, there are no pits on the reverse of the detector so all of the helium ions were below 43 MeV, which is shown by the detection limit point in Figure 1. There is a large error in both the energy and number of the longitudinal ions and it is possible there may be a further systematic error in the energy measurement due to the CR39 being off-axis. If the CR39 had been only 1 mm off axis then the maximum energy for the He^{2+} ions would change to (45 ± 14) MeV.

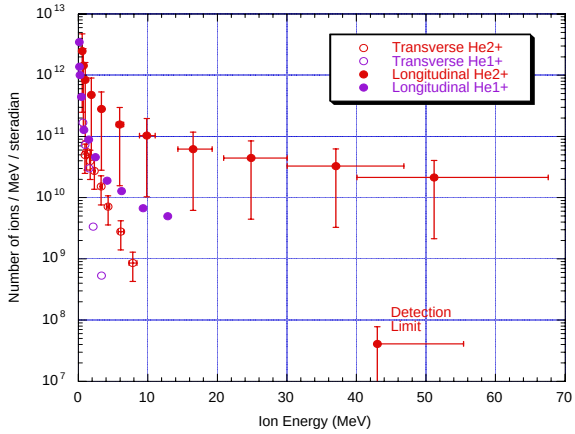

Figure 1. The transverse and longitudinal helium ion spectra.

PIC Simulations

The code OSIRIS[10] was used to perform two-spatial and three momentum dimensions (2D3V) particle-in-cell simulations of the interaction. The laser was propagated through a stationary box to allow the ion dynamics to be observed to later times, even after the laser pulse had passed through the plasma. In the longitudinal (x) direction, the box was 251 μm long with a resolution of 20.9 cells per λ and in the transverse (y) direction, the box was 251 μm wide with a resolution of 12.6 cells per λ. There was one electron and one ion per cell. The ion acceleration was investigated with changing plasma electron density.

Proton plasma, with a maximum density of $0.1n_c$, $0.05n_c$ or $0.01n_c$ were used, where n_c is the critical density. The plasma profile had a 70 μm long linear density ramp from vacuum to maximum density at the front of the plasma, 25 μm of plasma at maximum density and then 70 μm density ramp at the back into the vacuum. This kept the total amount of plasma the laser had to pass through the same. The vacuum then extended a further 84 μm behind the plasma.

Linearly polarised Gaussian-profiled pulses were used with duration of 500 fs (FWHM) and focused to a spot with a FWHM diameter of 8 μm at the top of the front density ramp to give an a_0 of 13.

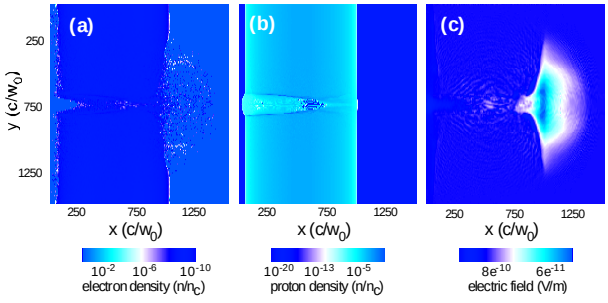

Figure 2. At a time 1.0 ps after the start of a simulation of a $0.05n_c$ density plasma (a) electron density, (b) proton density and (c) longitudinal electric field.

Firstly, the simulation of the $0.05n_c$ plasma is considered. Figure 2 shows (a) the electron and (b) the ion densities and (c) the longitudinal electric field at 1.0 ps after the start of the simulation. The electrons have moved out into the vacuum but the ions have not yet responded so a large electric field is formed at the plasma-vacuum interface.

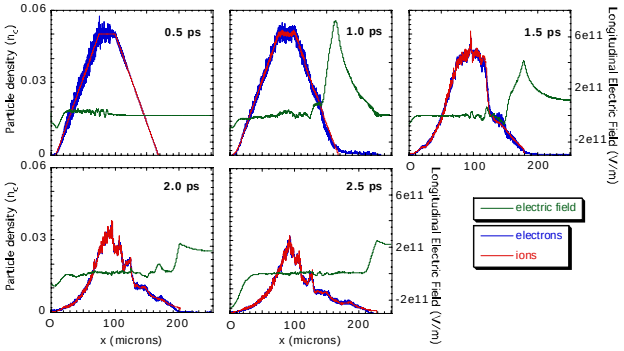

Figure 3. The progression of the electric field (green) with the electron (blue) and proton (red) movements at times of 0.5 ps, 1.0 ps, 1.5 ps, 2.0 ps and 2.5 ps for the $0.05n_c$ plasma density.

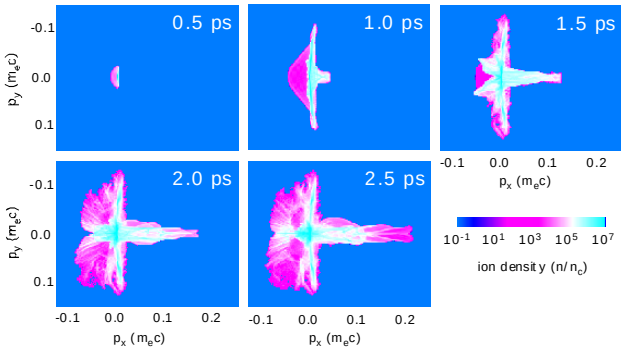

Figure 4. The proton momentum plots, p_x against p_y at times of 0.5 ps, 1.0 ps, 1.5 ps, 2.0 ps and 2.5 ps for the $0.05n_c$ plasma density.

As the electric field appears at the back of the density ramp, a proton beam is accelerated in the forward direction to a maximum energy of about 20 MeV and a divergence of 5° half angle. Figure 3 shows the progression of the longitudinal electric field in time with the movement of the electrons and ions from a 33 μm region around the centre of the box. At a time of 1.0 ps the electrons have started to move into the vacuum, whist the protons have yet to respond to the electric field. At 1.5 ps the ions have started to move out to neutralise the electric field and can been seen in the reduction of the peak intensity of the field.

Shown in Figure 4 are the proton momentum plots, p_x against p_y, at the corresponding times to the plots in Figure 3. Initially acceleration is only seen in the transverse direction p_y, as has been observed previously. But at 1.0 ps the ions start to be accelerated in the longitudinal direction, p_x, to form a collimated beam.

Figure 5 shows the peak longitudinal electric field from a 15 μm wide central region along the whole length of the x-direction of the box. Also plotted are the maximum longitudinal proton energies. This shows a smooth acceleration of the maximum energy protons from the time when the largest electric fields are seen, despite the peak electric field not decaying smoothly.

When simulating solid target proton and ion acceleration, one of the important parameters for the simulation grid to resolve is the plasma Debye length. The Debye length, λ_D, is given by $\lambda_D^2 = \varepsilon_0 k_B T_e / e^2 n_0$, where T_e is the electron temperature and n_0 is the plasma density. For very underdense plasma of around $0.05n_c$ the laser pulse is also present at the rear of the target

when the fast electrons are leaving. This means that the background plasma electron temperature is high (at 1.0 ps the temperature in the y direction is ~ 3 MeV). Consequently Using T_e = 3.0 MeV (found from simulation data at 1.0 ps) and the maximum plasma density as n_0 (at the vacuum interface the density will be much smaller, increasing the Debye length as $n_0^{1/2}$), the Debye length is approximately 2 μm. Therefore these simulations will be resolving the Debye length.

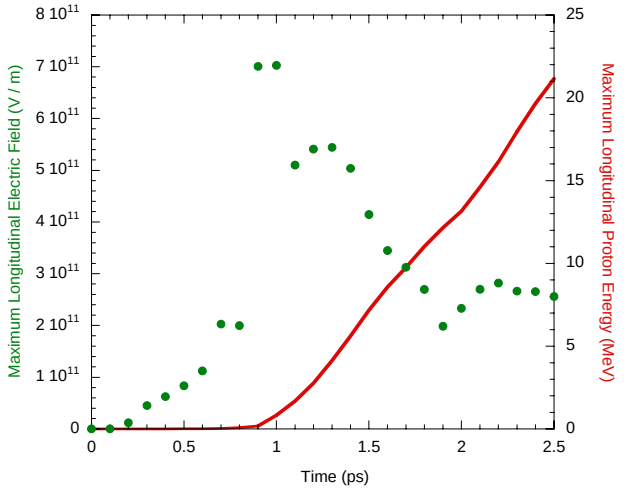

Figure 5. The time dependence of the peak longitudinal field and maximum proton energy for the 0.05n_c plasma density.

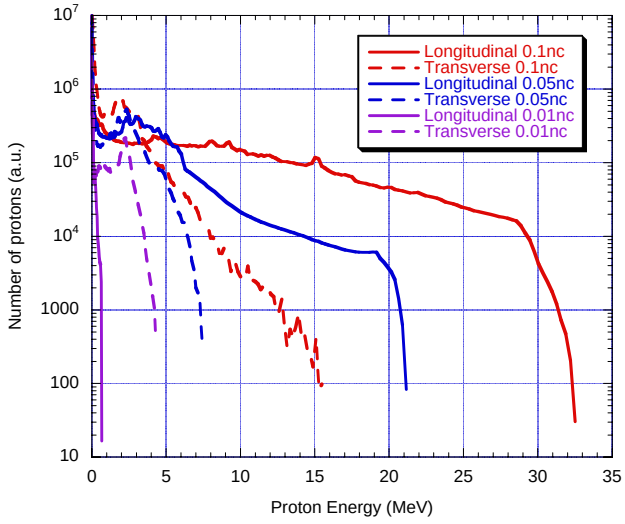

Figure 6. Simulated proton spectra at 2.5 ps for plasma densities of (a) 0.1n_c, (b) 0.05n_c and (c) 0.01n_c.

The simulated proton spectra, in both the longitudinal and transverse directions, for different density plasmas are shown in Figure 6. It shows that the longitudinal acceleration of the protons increases strongly with plasma density. At the lowest density of 0.01n_c, the transverse proton acceleration is more effective than the longitudinal acceleration whereas at the higher densities, the longitudinal acceleration is greatest.

The limitations of the simulations for representing the experiments are that the lengths of plasma in the simulations are very short compared with these experiments. The observation of the electric field accelerating the ions can only be made for as long as the ions remain in the box. The acceleration may continue for much longer than can be observed in the simulations. Also, the length of the density ramp at the back of the target plasma may be an important parameter and this too is much shorter in the simulations than it would be in the experiments.

Conclusions

Experimental results have been presented that show helium ions being accelerated to MeV energies in the longitudinal direction from underdense plasma interactions with the Vulcan Petawatt laser. Simulations show that this longitudinal ion acceleration is most efficient at high plasma densities and that they are likely to be emitted in a collimated beam. This longitudinal ion acceleration mechanism may provide a method for producing single species ion beams as an advantage over solid target ion acceleration where heavy ions are accelerated as well as protons.

Acknowledgements

The authors acknowledge the assistance of the Central Laser Facility staff at the Rutherford Appleton Laboratory in carrying out this work and MPQ Garching for their assistance with the analysis of the transverse ion data as well as the support of the UK Engineering and Physical Sciences Research Council (EPSRC). We gratefully acknowledge the OSIRIS consortium which consists of UCLA/IST (Portugal)/USC for the use of OSIRIS.

References

1. A Modena *et al.*, Nature 377, 606 (1995)
2. K Krushelnick *et al.*, Phys. Rev. Lett. 83, 737 (1999)
3. E Clark *et al.*, Phys. Rev. Lett. 84, 670 (2000); R Snavely *et al.*, Phys. Rev. Lett. 85, 2945 (2000)
4. G S Sarkisov *et al.*, Phys. Rev. E 59, 7042 (1999)
5. M S Wei *et al.*, Phys. Rev. Lett. 93, 155003 (2004)
6. M Roth *et al.*, Phys. Rev. Lett. 86, 436 (2001)
7. M Borghesi *et al.*, Phys. Plasmas 9, 2214 (2002)
8. F Pegoraro *et al.*, IEEE Trans. Plas. Sci. 28, 1177 (2000)
9. S P D Mangles *et al.*, Phys. Rev, Lett. 94, 245001 (2005)
10. R Hemker, Ph.D Thesis, UCLA (2000)